JMEPEG (2014) 23:294–301
DOI: 10.1007/s11665-013-0736-3

1059-9495/$19.00

Synthesis and Properties of La_2O_3-Doped 8 mol% Yttria-Stabilized Cubic Zirconia

Bulent Aktas, Suleyman Tekeli, and Serdar Salman

(Submitted June 7, 2013; in revised form August 15, 2013; published online October 8, 2013)

In this study, 8 mol% yttria-stabilized cubic zirconia (8YSZ) powder as a matrix material and 0-15 wt.% La_2O_3 powder as an additive were used to determine the effect of La_2O_3 addition and its amount on the phase stability, microstructure, sintering, and mechanical properties of 8YSZ. Colloidal processing was used to mix the powders uniformly and to obtain a homogenous microstructure. XRD results showed the existence of only a cubic crystal structure for 1 and 5 wt.% La_2O_3 addition amounts. However, $La_2Zr_2O_7$ with a hexagonal and cubic crystal structure was observed in 8YSZ specimens doped with 10 and 15 wt.% La_2O_3. Further, up to 5 wt.% La_2O_3 was completely dissolved in the crystal structure of the specimens; however, above 5 wt.%, La_2O_3 reacted with 8YSZ at high temperatures and formed pyrochloric $La_2Zr_2O_7$. Grain size measurements revealed that the grain size of 8YSZ increased up to 1 wt.% La_2O_3 addition, and then decreased beyond this amount. The hardness and fracture toughness of 8YSZ decreased and increased, respectively, with the increasing La_2O_3 amount.

Keywords fracture toughness (K_{IC}), hardness, La_2O_3, $La_2Zr_2O_7$, 8 mol% yttria-stabilized cubic zirconia (8YSZ)

1. Introduction

At atmospheric pressure and under equilibrium conditions, three polymorphic forms of zirconia are stable at different temperatures and composition ranges, namely, monoclinic, tetragonal, and cubic. Moreover, a high-pressure orthorhombic form of zirconia has also been reported (Ref 1). The successful production of zirconia bodies is not possible all the time owing to the large volume expansion associated with the martensitic tetragonal-monoclinic transformation. This phenomenon restricts the applications of zirconia, in spite of its excellent mechanical, electrical, and thermal properties. However, high-temperature polymorphs at room temperature can be made stable by the addition of suitable dopants. Fully stabilized cubic zirconia and partially stabilized tetragonal zirconia show interesting properties and are widely used as ionic conductors, coatings, and gas sensors in solid oxide fuel cells (SOFCs) and structural applications (Ref 2). The most frequently used dopants include Y_2O_3, CaO, MgO, and CeO_2, although other oxides such as those of rare-earth elements can also act as stabilizers for high-temperature structures. The incorporation of aliovalent cations to the lattice, thereby forming substitutional solid solutions, allows controlling the concentration of anionic vacancies in the microstructure. This aspect is particularly important while designing ionic conductors (Ref 3), and also plays an important role in the stabilization process (Ref 4). The process of stabilization with large-ionic-radius dopants is rationalized by the crystal chemistry model (Ref 5) that describes the dopant cations as typical stabilizers when they have a larger ionic size, lower charged state, and higher ionicity than Zr^{4+}. The ionic radii of Zr^{4+} and La^{3+} are 0.84 and 1.016 Å, respectively (Ref 6).

Pyrochlore $R_2Zr_2O_7$ (R = rare-earth metal) compounds have been used as hosts of fluorescence centers and oxidation catalysts. Therefore, many investigations have been carried out to study the electrical, optical, and catalytic properties of these materials (Ref 7-9). In particular, $La_2Zr_2O_7$, which is a pyrochlore compound, has been found to form at cathode $(La_{1-x}Sr_xMnO_3)$/electrolyte (ytrria-stabilized zirconia; YSZ) interfaces during high-temperature processing of SOFC (Ref 10, 11). $La_2Zr_2O_7$ compound has been synthesized in various studies by utilizing this phenomenon via methods including solid-state reaction (Ref 12, 13), nitric acid dissolution route, and sol-gel technique (Ref 12, 14, 15). The formation of pyrochlore $La_2Zr_2O_7$ compound was only achieved by sol-gel process (Ref 14). In addition to the possibility of stabilization of high-temperature structures, the ZrO_2-La_2O_3 system includes $La_2Zr_2O_7$ with a pyrochloric structure (Ref 16, 17). This compound finds applications as a catalyst (Ref 9) and thermal barrier (Ref 18). It can be synthesized by a solid-state reaction between oxides at 1500-1600 °C, or by the sol-gel process (Ref 14). Many studies on the La_2O_3-ZrO_2 system have been carried out. The phase stabilization and structure of nanocrystalline La_2O_3-ZrO_2 were studied by Thangadurai et al. (Ref 19). They prepared La_2O_3-doped nanocrystalline ZrO_2 by the chemical co-precipitation method with various dopant concentrations (3-30 mol%); further, they characterized the structural phases of the compounds by XRD. They reported that all specimens had a monoclinic phase. However, when the specimens were annealed at 1200 °C, the monoclinic phase emerged

Bulent Aktas, Engineering Faculty, Mechanical Engineering Department, Harran University, 63300 Sanliurfa, Turkey; **Suleyman Tekeli**, Technology Faculty, Metallurgical and Materials Engineering Department, Gazi University, 06500 Besevler-Ankara, Turkey; and **Serdar Salman**, Faculty of Engineering and Architecture, Mehmet Akif Ersoy University, Burdur, Turkey. Contact e-mails: baktas@harran.edu.tr, stekeli@gazi.edu.tr, and ssalman@marmara.edu.tr.

again with new cubic pyrochlore $La_2Zr_2O_7$ (Ref 19). Trombe and Foex (Ref 20) reported the existence of pyrochlore $La_2Zr_2O_7$ in the La_2O_3-ZrO_2 system for the La_2O_3 concentration of 15-30 mol% in ZrO_2. The effects of La_2O_3 addition on the phase transition and crystal growth of nanocrystalline $8La_2O_3$-8 mol% yttria-stabilized cubic zirconia (8YSZ) were investigated by Wang et al. (Ref 21). They reported that the crystal structure of $8La_2O_3$-8YSZ varied from a pure cubic phase to a mixture of cubic and pyrochlore dual phases when the calcination temperature was higher than 1000 °C, and that the volume fraction of pyrochlore $La_2Zr_2O_7$ increased with the increasing calcination temperature (Ref 21).

The objectives of this study were to improve the mechanical property (fracture toughness) of 8YSZ by La_2O_3 addition to make it suitable for use in SOFCs, and to investigate the synthesis and phase forms of La_2O_3-doped 8YSZ. 8YSZ is widely used as an oxygen sensor (Ref 9, 17), and as a solid electrolyte in SOFCs because of its high ionic conductivity (Ref 18). These applications require not only high conductivity but also high mechanical, chemical, and electrical stabilities (Ref 14). La_2O_3 was selected as a dopant for 8YSZ because of the mismatch between the ionic radii of ZrO_2 and La_2O_3, and because their valences are nearly equal. In addition, the reason for studying cubic zirconia (8YSZ) is that the ionic conductivity of 8YSZ is higher than that of tetragonal ZrO_2. Therefore, in the present study, the effects of various amounts of La_2O_3 addition on the phase equilibrium, microstructure, sintering, and mechanical properties of 8YSZ were investigated.

2. Experimental Procedure

In this study, 8YSZ (Tosoh, Japan) powders as a matrix material and La_2O_3 powders (Taimei, Japan) up to 15 wt.% as an additive were used. The average grain sizes were 0.3 μm for 8YSZ and 0.25 μm for La_2O_3. The chemical compositions of the powders used in the experiment are listed in Table 1.

The specimens for the microstructural and mechanical investigations were produced by means of colloidal processing. Doping was carried out in a plastic container by mechanical mixing of La_2O_3 up to 15 wt.% and 8YSZ powders with zirconia balls and ethanol. Mechanical mixing was performed in a "speks"-type mixer at 200 rpm for 12 h. The prepared slurries were left to dry for 24 h by leaving the lid in open condition. After the drying process, the agglomerated powders with medium hardness were ball milled for 10 min to obtain a good dispersion and to break-up the agglomerates. The powders obtained were sieved through a 60-μm sift and pressed under a 40-MPa pressure in a single-axis die with a radius of 10 mm and a height of 4 mm. The inner surface of the steel die was cleaned after each dry-pressing process, and stearic acid was applied to the side walls of the die. Sintering was carried out in a box-type furnace under normal atmospheric conditions. The pressed pellets were first subjected to a presintering process at 1000 °C, and were then sintered at temperatures between 1200 and 1550 °C for 1 h at heating and cooling rates of 5 °C/min. The density of the sintered specimens with perfect shapes was calculated using the rule of mixtures and obtaining their weight and volume ratio, which was determined by a geometric method. The relative density of the specimens was estimated by assuming that the sintered bodies had a cubic phase, and on the basis of the theoretical densities of 8YSZ and La_2O_3, i.e., 5.68 and 6.51 g/cm^3, respectively.

The surfaces of the specimens were ground and polished by a normal metallographic method after the sintering process, and the specimens were then thermally etched by keeping them in a furnace at 50 °C below the sintering temperature for 1 h. Microstructural investigation of the sintered specimens was performed using a scanning electron microscope (SEM, JEOL LV 6060). The grain sizes of the specimens were measured by the mean linear intercept method. Further, the average grain sizes of specimens were determined using the following equation:

$$D = \frac{L_i}{N_i \cdot M}, \quad \text{(Eq 1)}$$

where L_i is the length of the line, N_i is the number of grain-boundary intercepts, and M is the magnification in the photomicrograph of the material.

XRD (Shimadzu XRD 6000, CuK_α, $\lambda = 1.5405$ Å) was used to determine the probable changes in the crystal structure and lattice parameters of 8YSZ specimens doped with various amounts of La_2O_3. The specimens doped up to 15 wt.% La_2O_3 were tested in the scan span 0-70° at a scan speed of 0.03, and the diffraction angles were measured. The lattice parameters were evaluated for each composition by using these diffraction angles.

Both hardness and fracture toughness values of the specimens were determined using a Vickers hardness tester under a load of 2 kg and duration of 15 s. Hardness values were calculated using the following equation:

$$H_v = 1854\,P/d^2, \quad \text{(Eq 2)}$$

where P is the applied load (kg), and d is the mean value of the diagonal length (mm). Fracture toughness values were calculated by measuring the length of cracks that formed on the edges of the track as a result of hardness tests. Cracks were measured immediately after applying the load on the specimen so that they would not be affected by environmental factors. Fracture toughness was calculated using the "half-penny-crack" formula as suggested by Anstis et al. (Ref 22):

$$K_{IC} = 0.016(E/H_v)^{1/2}\left(P/C^{3/2}\right), \quad \text{(Eq 3)}$$

where E is the Young modulus, H_v is the Vickers hardness, P is the applied load, and C is the crack length.

Table 1 The chemical compositions of the powders used in the experimental works

	wt.%								
Powders	**ZrO_2**	**Y_2O_3**	**La_2O_3**	**TiO_2**	**FeO_2**	**Na_2O_3**	**CaO**	**Al_2O_3**	**SiO_2**
8YSZ	85.9	13.6	···	0.1	0.003	0.01	0.02	0.25	0.1
La_2O_3	···	···	99.99	···	0.003	···	0.005	···	0.002

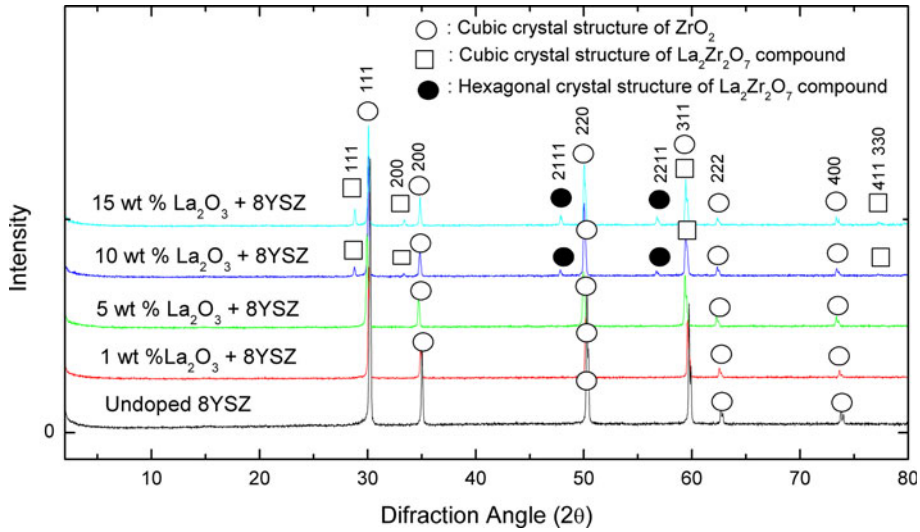

Fig. 1 XRD patterns of undoped and La_2O_3-doped 8YSZ specimens

3. Experimental Results and Discussion

XRD patterns for 8YSZ specimens doped with various amounts of La_2O_3 are shown in Fig. 1. XRD results showed that the specimens containing 1 and 5 wt.% La_2O_3 were composed of only a cubic crystal structure. Further, these specimens showed no La_2O_3 peaks, indicating that La_2O_3 was completely dissolved in the 8YSZ matrix and did not remain as a secondary phase around the grains and grain boundaries of 8YSZ. However, when more than 5 wt.% La_2O_3 was added, peaks corresponding to pyrochloric $La_2Zr_2O_7$ emerged, showing that overdoped La_2O_3 was not solubilized in the 8YSZ matrix and formed a secondary phase of $La_2Zr_2O_7$ at high temperatures. Trombe et al. (Ref 20) reported that $La_2Zr_2O_7$ phase occured in the concentration of La_2O_3 between 15 and 30%. SEM and EDS analyses revealed that this new phase preferentially precipitated around the grains and grain boundaries of 8YSZ. Further, XRD results showed that $La_2Zr_2O_7$ was composed of hexagonal and cubic crystal structures. Some of the peaks of the 8YSZ specimens doped with 10 and 15 wt.% La_2O_3 can be indexed to cubic-pyrochlore-structured $La_2Zr_2O_7$ and hexagonal-crystal-structured $La_2Zr_2O_7$, which result is in agreement with JCPDS 30-1468 and JCPDS 17-0450 (International Center for Diffraction Data Files). Further examination of the XRD peaks of the 8YSZ specimens doped with 10 and 15 wt.% La_2O_3 revealed that the cubic-pyrochlore-structured $La_2Zr_2O_7$ phase existed in (111), (200), (311), (411), and (330) crystal planes, and the hexagonal-crystal-structured $La_2Zr_2O_7$ phase existed in (3211), (2111), and (2211) crystal planes. The formation of pyrochloric $La_2Zr_2O_7$ was due to the difference in the ionic radii and crystal structures of La^{3+} and Zr^{4+} ions. As is known, the ionic radius of La^{3+} with a hexagonal structure is 1.016 Å and that of Zr^{4+} with a cubic crystal structure is 0.84 Å. The pyrochloric structure is defined as two distinct and intertwined structures. These two structures are distinguished as a cation centered of octahedral ZrO_6. An anion-cantered layout of tetrahedral La_4O. $La_2Zr_2O_7$ is formed by the unification of two octahedral and one tetrahedral structure, with La^{3+} cations being situated in a hexagonal window of the octahedral lattice (Ref 23, 24). The effect of La_2O_3 addition on the lattice

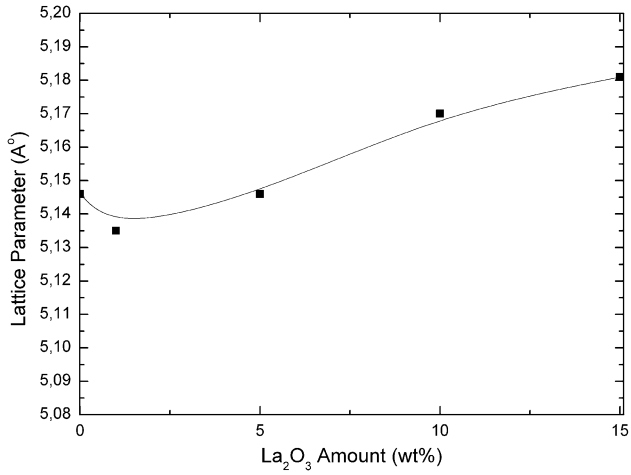

Fig. 2 Lattice parameter variation of the 8YSZ with La_2O_3 content

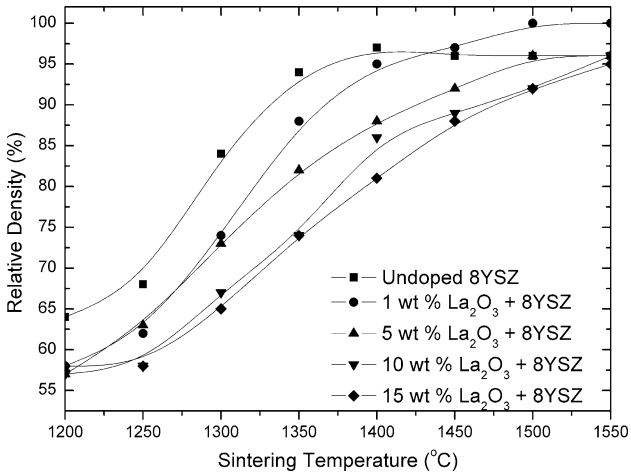

Fig. 3 Relative density of the 8YSZ specimens doped with different amounts of La_2O_3, sintered at various temperatures for 1 h

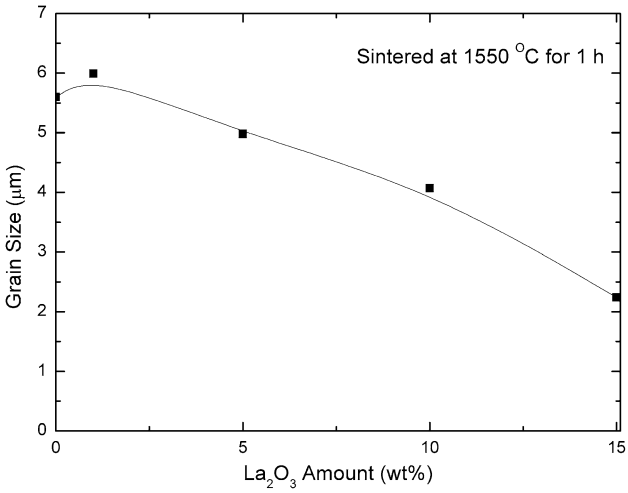

Fig. 4 Grain size variation of the 8YSZ with La_2O_3 amount

parameter of 8YSZ is shown in Fig. 2. The lattice parameters of all the specimens were obtained by applying Cohen's method (Ref 25). Thangadurai et al. (Ref 26) reported that the lattice parameter of ZrO_2 doped with 3-30 mol% La_2O_3 varied between 5.14 and 5.23 Å. In this study, the lattice parameter of undoped 8YSZ was 5.146 Å, and it increased to 5.181 A upon the addition of 15 wt.% La_2O_3. Thus, the mean lattice parameter of 8YSZ increased upon La_2O_3 addition. This increase in the lattice parameter, which corresponds to Vegard's rule, can be attributed to the replacement of La^{3+} ions by Zr^{4+} and Y^{3+} ions in the cubic crystal of 8YSZ. In other words, La^{3+} ions, the ionic radius of which is 20% larger than that of Zr^{4+}, increased the lattice parameter of 8YSZ.

The effects of La_2O_3 addition and its amount on the sinterability of 8YSZ are shown in Fig. 3. La_2O_3-doped 8YSZ specimens were pressureless sintered at various temperatures for 1 after presintering at 1000 °C. The results showed that the relative density of the specimens increased with the increasing sintering temperature and decreased with the increasing La_2O_3

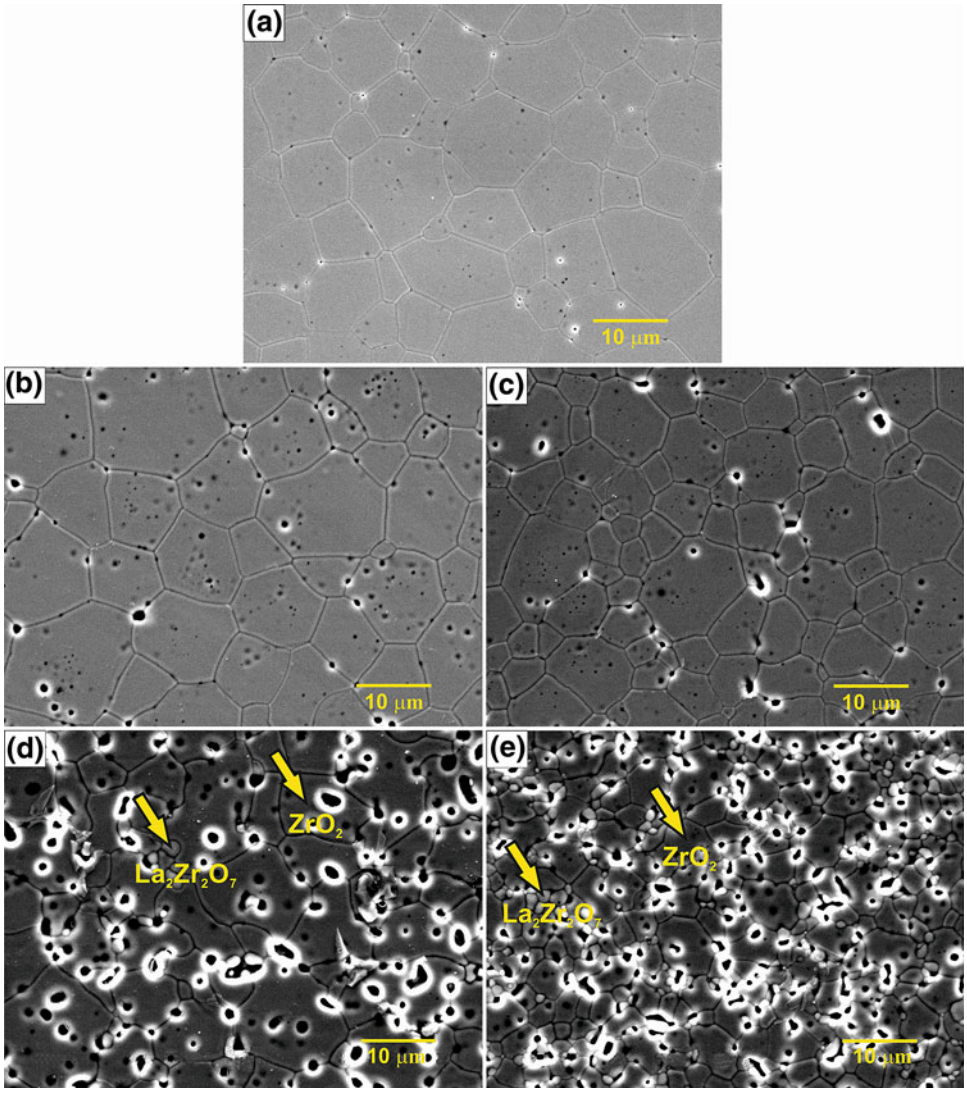

Fig. 5 SEM micrographs of the thermally etched specimens with (a) undoped, (b) 1 wt.%, (c) 5 wt.%, (d) 10 wt.%, and (e) 15 wt.% La_2O_3-doped 8YSZ specimens sintered at 1550 °C for 1 h

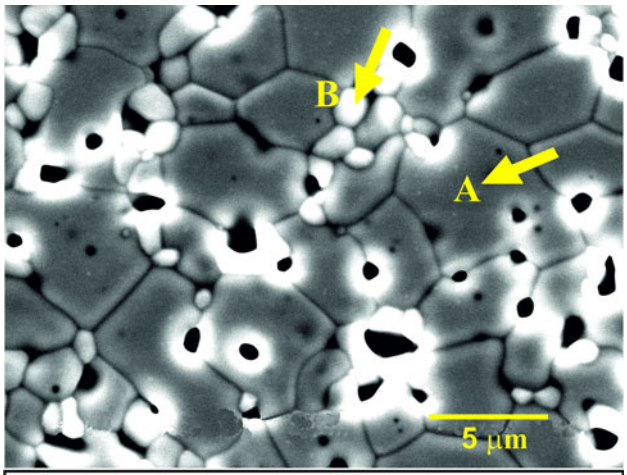

wt %				
EDS analysis points	Zr^{4+}	La^{3+}	Y^{3+}	O^{2-}
A	63.5	6.43	13.29	16.71
B	42.9	37.06	4.58	15.35

Fig. 6 EDS results of 15 wt.% La_2O_3-doped 8YSZ specimen sintered at 1550 °C for 1 h

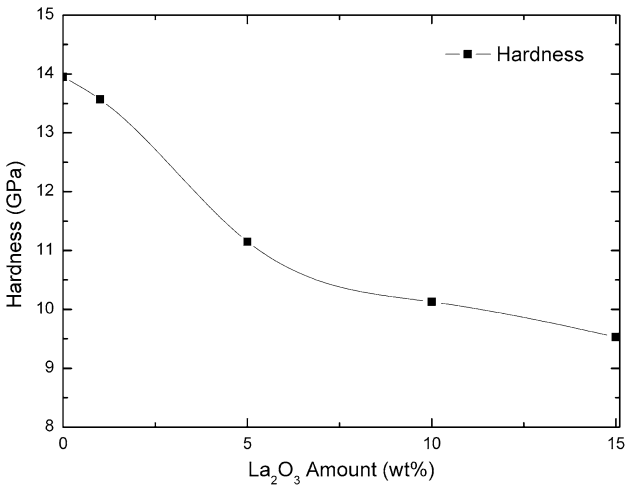

Fig. 7 Effect of La_2O_3 amount on the hardness of 8YSZ specimens sintered at 1550 °C for 1 h

amount at all temperatures. This decrease in the relative density was due to the porosities in the main matrix and around the grain boundaries, especially when the amount of La_2O_3 doping was high. Moreover, $La_2Zr_2O_7$, which was formed in 8YSZ specimens doped with high amounts of La_2O_3 at high temperatures and precipitated at the grain boundaries, prevented 8YSZ grains from touching each other and thus slowed the diffusion rate of the atoms at the grain boundaries as a result of an increase in the grain boundary diffusion; this could be another reason for the decrease in relative density. The change in the grain size with La_2O_3 amount is shown in Fig. 4. It can be seen from this figure that, up to 1 wt.% La_2O_3 addition

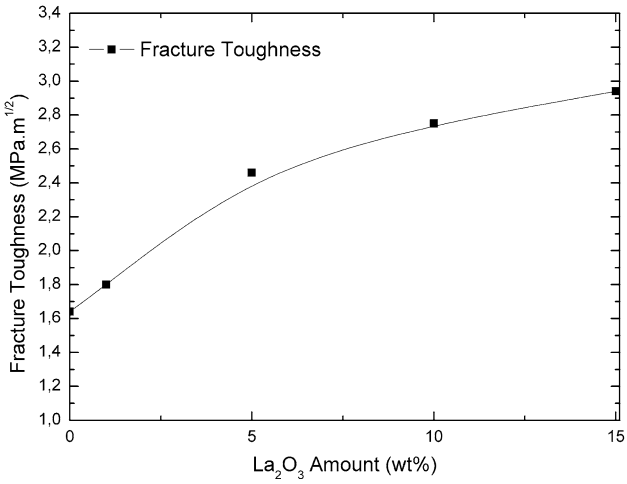

Fig. 8 Effect of La_2O_3 amount on the fracture toughness of 8YSZ specimens

increased the grain size. Intergranular phases with the highest solubility would have the lowest viscosity at high temperatures and highest diffusivity (Ref 27). Thus, the increase in the grain size of 8YSZ with the addition of 1 wt.% La_2O_3 could be due to the complete dissolution of La_2O_3 in the 8YSZ structure, thereby providing an easy diffusion path at grain boundaries. However, further increase in the La_2O_3 content led to a decrease in the grain size. This decrease in the grain size can be explained by the fact that pyrochloric $La_2Zr_2O_7$, which is formed around and at the grain boundaries in 8YSZ at high temperatures, increased the grain boundary cohesive resistance by the pinning effect, and thus, the grain boundary mobility and energy decreased.

The microstructures of the specimens doped with various amounts of La_2O_3 after sintering at 1550 °C for 1 are shown in Fig. 5. The undoped 8YSZ specimens and those doped with 1 and 5 wt.% La_2O_3 have a equiaxed, faceted, uniform, and coarse-grained structures (Fig. 5a-c). The microstructures of the 8YSZ specimens doped with 10 and 15 wt.% La_2O_3, on the other hand, have faceted 8YSZ grains together with round and smaller $La_2Zr_2O_4$ grains (Fig. 5d, e). Further, it can be observed in Fig. 5 that the porosity level increased with the increasing La_2O_3 content. The EDS analysis results for different parts of an 8YSZ specimen doped with 15 wt.% La_2O_3 are shown in Fig. 6. While the amount of La^{3+} ions in the 8YSZ grains (point A) was 6.43 wt.%, this rate was 37.06 wt.% in the secondary-phase $La_2Zr_2O_4$ grains (point B). EDS results showed that this phase around the grains and grain boundaries of 8YSZ belonged to $La_2Zr_2O_4$.

The hardness values of the 8YSZ specimens doped with various amounts of La_2O_3 after sintering at 1550 °C for 1 shown in Fig. 7. The results showed that the hardness of the specimens decreased as the La_2O_3 doping amount increased. The decrease in hardness might be due to the difference between hardness and Young's modulus of pyrochloric $La_2Zr_2O_7$ and 8YSZ. Another reason may be the increasing porosity level with the increasing amount of La_2O_3 doping. The porosity dependence on hardness has been studied intensively. In general, hardness decreases with porosity (Ref 28). The effect of La_2O_3 doping amount on the fracture toughness of 8YSZ is shown in Fig. 8. The fracture toughness of the 8YSZ

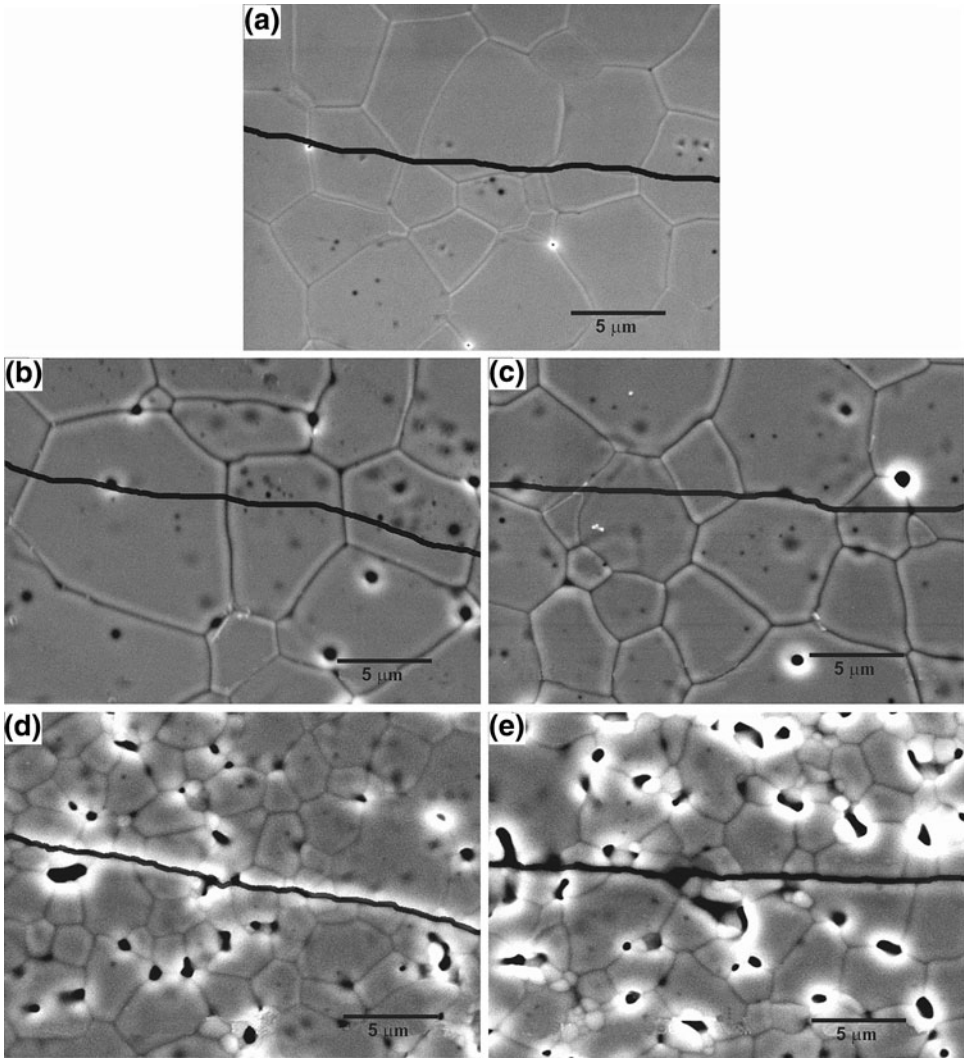

Fig. 9 SEM micrographs of crack propagation modes (a) undoped, (b) 1 wt.%, (c) 5 wt.%, (d) 10 wt.%, and (e) 15 wt.% La_2O_3-doped 8YSZ specimens sintered at 1550 °C for 1 h

specimens increased with the increasing La_2O_3 doping amount. The increase in the fracture toughness can be explained by the decrease in the grain size of 8YSZ as a result of La_2O_3 addition. Materials with smaller grains tend to have higher fracture toughness. Cracks propagate either along the grain boundaries or inside the grains. New surfaces form when grains split. The formation of new surfaces results in greater surface energy and higher fracture toughness. Therefore, fracture toughness can be controlled by controlling the grain size. Another reason for the high fracture toughness of the La_2O_3-doped 8YSZ specimens is the presence of pyrochloric $La_2Zr_2O_7$ around the grains and grain boundaries of 8YSZ. As is known, pyrochloric $La_2Zr_2O_7$ formed when the doping amount of La_2O_3 was greater than 5 wt.% $La_2Zr_2O_7$ around the grains, and grain boundaries of 8YSZ caused the cracks to deflect, thereby leading to an increase in the fracture toughness of the specimens. Crack propagation modes observed in undoped 8YSZ specimens and those doped with various amounts of La_2O_3 are shown in Fig. 9. As observed in this figure, cracks propagated straight through the 8YSZ grains, i.e., the transgranular fracture mode appeared in the undoped 8YSZ specimens and those doped with 1 and 5 wt.% La_2O_3. However, cracks were deflected by the $La_2Zr_2O_7$ grains in the 8YSZ specimens doped with 10 and 15 wt.% La_2O_3. This deflection was the reason for the increase in the fracture toughness of the specimens. The deflection was caused by residual stresses due to the difference between Young's modulus and the coefficient of thermal expansion of 8YSZ and $La_2Zr_2O_7$ grains. In general, cracks propagate between grains if their thermal expansion coefficient is smaller than that of the reinforcing member (Ref 29).

Figure 10 shows the SEM micrographs of the cracks generated by an indentation load of 2 kg applied for a duration of 15 s. It should be noted that cracks emanate from the corners of the indents and that crack lengths differed according to the La_2O_3 content. For the undoped 8YSZ specimen, indents with long crack lengths were observed. On the contrary, with an increase in the La_2O_3 doping amount, crack lengths decreased (Fig. 11). The increase in the fracture toughness and the decrease in the crack length in specimens with high amounts of La_2O_3 doping could be attributed to the smaller grain size of the specimens and the presence of $La_2Zr_2O_7$ at the grain boundaries causing crack deflection.

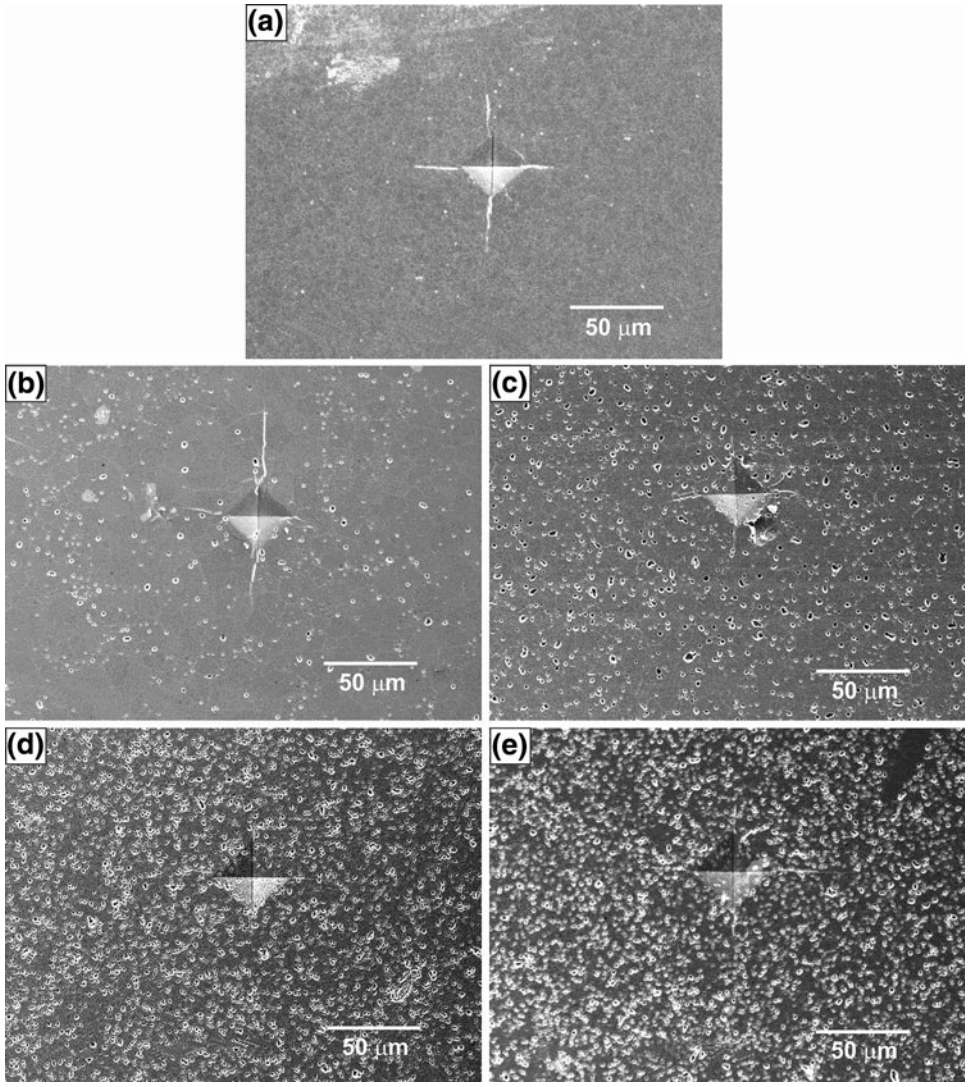

Fig. 10 SEM micrographs of Vickers indentations with different crack lengths (a) undoped, (b) 1 wt.%, (c) 5 wt.%, (d) 10 wt.%, and (e) 15 wt.% La_2O_3-doped 8YSZ specimens sintered at 1550 °C for 1 h

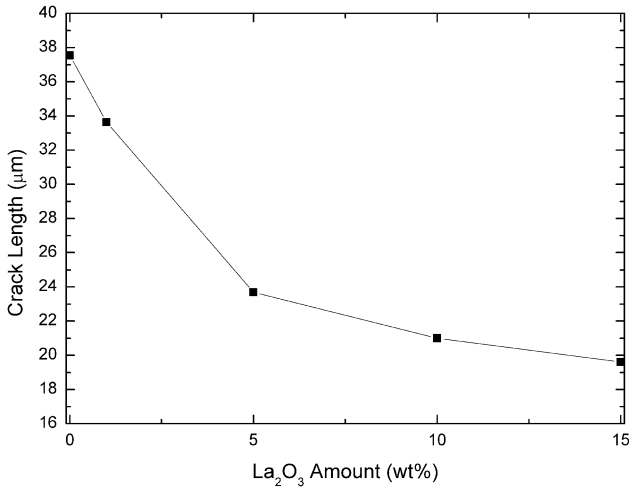

Fig. 11 Effect of La_2O_3 amount on the crack length of 8YSZ specimens

4. Conclusions

(1) XRD results showed that the 8YSZ specimens doped with 1 and 5 wt.% La_2O_3 had cubic crystal structures, and their structures did not change with the addition of La_2O_3. Further, the specimens doped with 1 and 5 wt.% La_2O_3 revealed no La_2O_3 peaks, indicating that La_2O_3 was completely dissolved in the 8YSZ matrix and did not remain in the specimens as a secondary phase around the grains and grain boundaries of 8YSZ. However, when the doping amount of La_2O_3 was increased to more than 5 wt.%, peaks corresponding to pyrochloric $La_2Zr_2O_7$ emerged, showing that overdoped La_2O_3 was not solubilized in the 8YSZ matrix and formed a secondary phase of $La_2Zr_2O_7$ at high temperatures.

(2) The relative density of the 8YSZ specimens decreased as the La_2O_3 doping amount increased. This decrease was probably due to the presence of pyrochloric $La_2Zr_2O_7$, which precipitated at the grain boundaries at high

temperatures, and also due to the porosities observed in the specimens with high La_2O_3 content.

(3) The grain size of 8YSZ specimens increased at 1 wt.% La_2O_3 addition and further increase in the La_2O_3 content ($\geq$ 5 wt.%) resulted in decrease in the grain size. These results indicate that La_2O_3 addition within the solubility limit accelerated grain growth. The decrease in the grain size can be explained by the fact that the secondary phase of pyrochloric $La_2Zr_2O_7$, which was formed at the grain boundaries at high temperatures, increased the grain boundary cohesive resistance, and thus, limited the grain boundary mobility and energy.

(4) The hardness of the La_2O_3-doped 8YSZ specimens decreased with the increasing La_2O_3 doping amount. This decrease in the hardness might be due to the difference between the hardness and Young's modulus values of pyrochloric $La_2Zr_2O_7$ and 8YSZ grains. Another reason may be the increasing porosity due to the increase in the La_2O_3 doping amount.

(5) Fracture toughness of the La_2O_3-doped 8YSZ specimens increased with the doping amount. $La_2Zr_2O_7$, which is small grained and is formed at the grain boundaries, was one of the main causes of this increase in fracture toughness.

Acknowledgments

The authors thank Gazi University and Marmara University, Turkey, for the provision of laboratory facilities.

References

1. L.K. Lenz and A.H. Heuer, Stress-Induced Transformation During Subcritical Crack Growth in Partially Stabilized Zirconia, *J. Am. Ceram. Soc.,* 1982, **65,** p C-192–194
2. R. Stevens, *Introduction to Zirconia*, Magnesium Electron Ltd., Manchester, 1986
3. S.P.S. Badwal, Ceramic Superionic Conductors, *Materials Science and Technology—A Comprehensive Treatment*, R.W. Cahn, P. Haasen, and E.J. Kramer, Ed., VCH Publishers, New York, 1994, p 567–588
4. P. Li and I.W. Chen, Effect of Dopants on Zirconia Stabilization—An X-ray Absorption Study I, Trivalent Dopants, *J. Am. Ceram. Soc.*, 1994, **77**, p 118–128
5. S.M. Ho, On the Structural Chemistry of Zirconium Oxide, *Mater. Sci. Eng.*, 1982, **54**, p 23–29
6. R.C. Weast and M.J. Astle, *CRC Handbook of Chemistry and Physics*, CRC Press, Boca Raton, 1981
7. H. Otaki, H. Kido, T. Hoshikawa, M. Shimada, and M. Koizumi, Crystal Structure and Fluorescence Properties of $R_2Zr_2O_7$ and $(R_{1-l}E_{\sim x})ZO_7$ Compounds, *Nippon Seram. Kyo. Gak.*, 1988, **96**, p 124–126
8. R.A. McCauley, Infrared-Absorption Characteristics of the Pyrochlore Structure, *J. Opt. Soc. Am.*, 1973, **63**, p 721–725
9. S.J. Korf, H.J.A. Koopmans, B.C. Lippens, A.J. Burggraaf, and P.J. Gellings, Electrical and Catalytical Properties of Some Oxides with the Fluorite and Pyrochlore Structure, *J. Chem. Soc. Faraday Trans. I*, 1987, **83**, p 1485–1491
10. J. Echigova, T. Ohfuji, and H. Suto, Preparation of La_2NiO_4 Films by d.c. Sputtering on Cubic ZrO_2, *J. Mater. Sci. Lett.*, 1994, **13**, p 1098–1100
11. T. Setoguchi, T. Inoue, H. Takebe, K. Eguchi, K. Morinaga, and H. Arai, Fabrication and Evaluation of Flat Thick Film Type Solid Oxide Fuel Cell, *Solid State Ion.*, 1990, **37**, p 217–221
12. F.W. Poulsen and N. Puil, Phase Relations and Conductivity of Sr and La-Zirconates, *Solid State Ion.*, 1992, **53**(56), p 777–783
13. J.A. Labrincha, F.M.B. Marques, and J.R. Frade, $La_2Zr_2O_7$ Formed at Ceramic Electrode/YSZ Contacts, *J. Mater. Sci.*, 1993, **28**, p 3809–3815
14. H. Kido, S. Komarneni, and R. Roy, Preparation of $La_2Zr_2O_7$ by Sol-Gel Route, *J. Am. Ceram. Soc.*, 1991, **74**, p 422–424
15. Y. Matsumura, M. Yoshinaka, K. Hirota, and O. Yamaguchi, Formation and Sintering of $La_2Zr_2O_7$ by the Hydrazine Method, *Solid State Commun.*, 1997, **104**, p 341–345
16. S.J. Schneider, R.S. Roth, and J.L. Waring, Solid-State Reactions Involving Oxides of Trivalent Cations, *J. Res. Natl. Bur. Stand. A*, 1961, **65A**, p 345–354
17. A. Rouanet, Zirconium Dioxide-Lanthanide Oxide Systems Close to the Melting Point, *Rev. Int. Hautes Temp. Refract.*, 1971, **8**, p 161–180
18. X.Q. Cao, R. Vassen, W. Jungen, S. Schwartz, F. Tietz, and D. Stover, Thermal Stability of Lanthanum Zirconate Plasma-Sprayed Coating, *J. Am. Ceram. Soc.*, 2001, **84**, p 2086–2090
19. P. Thangadurai, A.C. Bose, and S. Ramasamy, Phase Stabilization and Structural Studies of Nanocrystalline La_2O_3-ZrO_2, *J. Mater. Sci.*, 2005, **40**(15), p 3963–3968
20. F. Trombe and M. Foex, *CR Acad. Sci.*, 1951, **233**, p 254
21. C. Wang, Y. Wang, Y. Cheng, L. Zhu, B. Zou, Y. Zhao, W. Huang, X. Fan, Z.S. Khan, and X. Cao, Synthesis of Nanocrystilline La_2O_3-Y_2O_3-ZrO_2 Solid Solutions by Hydrothermal Method: A Crystal Growth and Structural Study, *J. Cryst. Growth*, 2011, **335**, p 165–171
22. G.R. Anstis, P. Chantikul, B.R. Lawn, and D.B. Marshall, A Critical-Evaluation of Indentation Techniques for Measuring Fracture-Toughness Strength Method, *J. Am. Ceram. Soc.*, 1981, **64**, p 533–543
23. B.G. Hyde, J.G. Thompson, and R.L. Withers, Crystal Structures of Principal Ceramic Materials, *Mater. Sci. Technol. A*, 1994, **11**, p 35
24. M.C. Fuertes and J.M. Porto Lopez, Mechanochemical Synthesis and Thermal Evolution of La^{3+}-ZrO_2 Cubic Solid Solutions, *Ceram. Int.*, 2004, **30**, p 2137–2142
25. M.U. Cohen, Precision Lattice Constants from X-ray Powder Photographs, *Rev. Sci. Instrum.*, 1935, **6**, p 68
26. P. Thangadurai, V. Sabarinathan, A. Chandra Bose, and S. Ramasamy, Conductivity Behaviour of a Cubic/Tetragonal Phase Stabilized Nanocrystalline La_2O_3-ZrO_2, *J. Phys. Chem. Solids*, 2004, **65**, p 1905–1912
27. A.A. Sharif, P.H. Imamura, T.E. Mitchell, and M.L. Mecartney, Control of Grain Growth Using Intergranular Silicate Phases in Cubic Yttria Stabilized Zirconia, *Acta Mater.*, 1998, **46**(11), p 3863–3872
28. J. Luo and R. Stevens, Porosity-Dependence of Elastic Moduli and Hardness of 3Y-TZP Ceramics, *Ceram. Int.*, 1999, **25**(3), p 281–286
29. W. Shanghua, "Influence of Crack Path on Fracture Toughness of Ceramic Matrix Composites," Ph.D. thesis, University of Alabama, Tuscaloosa, 2001